

Received April 4, 2022, accepted April 17, 2022, date of publication April 22, 2022, date of current version May 4, 2022.

Digital Object Identifier 10.1109/ACCESS.2022.3169778

A Transcutaneous Fetal Visual Stimulator

KARTHIKEYAN KALYANASUNDARAM BALASUBRAMANIAN¹, (Member, IEEE),
FRANCESCO DIOTALEVI¹, CLAUDIO LORINI¹, ANDREA CAVALLO^{2,3},
NOVELLA PRETTI^{2,3}, DARIO PALADINI⁴, DIEGO TORAZZA⁵, CRISTINA BECCHIO^{3,6},
AND MARCO CREPALDI¹, (Member, IEEE)

¹Electronic Design Laboratory (EDL), Istituto Italiano di Tecnologia, 16152 Genoa, Italy

²Department of Psychology, University of Turin, 10124 Turin, Italy

³Cognition Motion and Neuroscience (CMON), Istituto Italiano di Tecnologia, 16152 Genoa, Italy

⁴Fetal Medicine and Surgery Unit, Istituto Giannina Gaslini, 16147 Genoa, Italy

⁵Robotics Brain and Cognitive Sciences (RBCS), Istituto Italiano di Tecnologia, 16152 Genoa, Italy

⁶Department of Neurology, University Medical Centre Hamburg-Eppendorf, 20251 Hamburg, Germany

Corresponding author: Karthikeyan Kalyanasundaram Balasubramanian (karthikeyan.kalyanasundaram@iit.it)

This work involved human subjects or animals in its research. Approval of all ethical and experimental procedures and protocols was granted by the Comitato Etico Regionale della Regione (39/2020) the Italian Ministry of Health under Protocol No. 45831.

ABSTRACT An infant's brain effortlessly acquaints to a motion. Fetuses in the third trimester of pregnancy can also exhibit similar capacity, but further investigations on this matter are needed. Literature studies have assessed fetal response to visual stimulus experiments, but the known setups are reinforced with fixed illumination points and cannot be used to render generic motion visually. This work presents a system to overcome this limitation, i.e., provide dynamic motion as a visual stimulus for fetuses in the third trimester of pregnancy when they can process visual stimulus, and thus biological motion can be used for assessing fetal reactions. Our Transcutaneous Fetal Visual Stimulator (TCFVS) uses two high-resolution LED arrays (16 × 20), a reconfigurable SoC (Xilinx FPGA and ARM core), and intuitive software to provide flexible control and ease of operation analyzing fetal reactions in response to visual stimulation. The paper details the TCFVS hardware and software architecture and presents benchmarks on the software toolchain to import generic patterns or motion capture in the visual stimulation domain. Our ad-hoc pixel remapping technique, an important component to precisely visualize stimulations in our hardware, is necessary and results in higher performance with respect to conventional downscaling techniques. To provide the first validation of our device in view of a systematic study, we verified real fetus movements when stimulated with TCFVS.

INDEX TERMS TCFVS, biomedical SoC, fetal behavior, fetal eye movement, fetal head movement.

I. INTRODUCTION

Inherent barriers to delivering visual stimuli to the fetus in-utero have hindered progress in fetal visual research [1]. As a result, little is known about fetal visual capacities and preferences and the possibility of transnatal transmission in the visual domain. In a recent study, Reid *et al.* investigated the possibility of a fetal visual preference for face stimuli [2]. Newborns prefer looking at faces over other shapes, and this preference extends to schematic face patterns [3]. Projecting three dots of light in a face configuration through the abdominal wall, Reid *et al.* documented a similar preferential

The associate editor coordinating the review of this manuscript and approving it for publication was Abdallah Kassem¹.

tracking of faces in fetuses at 33 to 36 gestational weeks. Specifically, fetuses performed more head turns to face configuration stimuli presented in an upright orientation than to identical stimuli presented in an inverted orientation.

The capacity (i) to present visual stimuli through projected light and (ii) to precisely measure fetal behavior using ultrasound recordings allows in principle for studies with the human fetus that closely resemble postnatal methodologies with infant populations. However, the conduct of such studies has been so far limited by the lack of a suitable technology to deliver visual stimuli with perceptual content to the fetus. Reid *et al.* assembled three laser diodes in a face configuration. However, the presentation of more complex shapes and objects may not be possible with this approach [4]. Moreover,



FIGURE 1. Transcutaneous Fetal Visual Stimulator. The device, FPGA-based and full-custom designed, comprises two displays that render complex visual patterns to fully cover the womb while enabling fetal measurements using an Ultrasound probe.

this approach does not permit the presentation of dynamic stimuli. This limits the experimental paradigm that can be studied, including paradigms that aim to investigate the perception of biological motion. This area is of special interest to fetal vision research as humans demonstrate a preference for biological over non-biological motion, and this preference is present at birth [5]. Here we describe a transformative technology - Transcutaneous Fetal Visual Stimulator (TCFVS) – that can be used to project static and dynamic visual stimuli to the fetus (see Fig. 1).

TCFVS is (i) a non-invasive platform that presents both static and dynamic visual stimuli in the forms of red light to the fetuses, (ii) a collection of software tools that provides the experimenter the flexibility of choosing or changing the visual stimulus during an experiment and import stimuli from a VICON system, and (iii) a specific hardware stimulator that allows the experimenters to easily apply visual stimulation through the mothers' wombs as long as the fetal face is oriented towards the front of the mother. Moreover, in this paper, we address the methods to render motion, especially biological motion. TCFVS opens up new possibilities in fetal visual research. The remainder of this paper is as follows. The TCFVS system design, the data, and the control path with their detailed operation are discussed in Sec. II. Sec. III details the stimulus generation and pattern reconstruction techniques, and Sec. IV represents algorithm validation and comparative results. Sec. V discusses the TCFVS system performance showing qualitative clinical observation results obtained on a first test set-up, and finally, Sec. VI concludes the paper.

II. TRANSCUTANEOUS FETAL VISUAL STIMULATOR SYSTEM DESIGN

A. DESIGN REQUIREMENTS

We determined design requirements by preliminary interviewing clinicians and experimenters and then testing

the prototype design within the intended environment. Feedback and suggestions received during validation were directly incorporated into the prototype TCFVS and introduced to users. This interactive experience allowed users to see their modifications, leading to additional detailed feedback across sessions. Design requirements included user needs, product description, regulatory standards, functional requirements, performance and physical requirements, human-system interfacing.

Well-defined user needs to create the basis for design inputs. A compact, compliant, and flexible multi-array display was considered as a primary prerequisite for generating a visual stimulus for fetuses. The device must have a display size big enough to be used in experiments ($\sim 10 \times 10$ cm), and it shall include stereo functionality, that is, the capability of showing images on two different displays simultaneously. In light of not knowing the fetus positioning, it is thus necessary to provide a wide display aperture. The device shall be adept to the real-time configuration for visualizing both static image and dynamic motion (a pattern/s moving at a constant velocity or a biological velocity), ad-hoc processed to enable a high contrast and precise visualizing. Considering the variable thickness of the maternal abdominal tissue and the variability that may be found from one subject to another, it is thus necessary that the system display visual stimuli, for instance, by adjusting intensity or grouping multiple light sources to modulate intensity. In terms of illumination, the current state-of-the-art displays used for consumer electronics are not suitable for implementing such visual stimulator, mainly because they cannot provide a very high on/off static contrast that may be possible using a dedicated LED dot matrix (on the order of 1000:1).

In terms of power supply requirements, up to date (unless future versions of the system to be used, for instance, as aids for periodical stimulation at home), there are no particular requirements in terms of power consumption of the device, provided that safety is guaranteed and that the displays never generate heat even when attached to the skin. Considering an intended use as equipment in a hospital environment, it is not required that the device operates wirelessly. Rather it is required to use cable connections. This enables the release of available wireless spectrum for life-critical equipment. The device can be controlled using an external personal computer, and it is required that the operator can control the device at a maximum distance of 2 m from the subjects. Considering the biological movements to be displayed on the Stimulator shall be acquired directly from real biological motion, it is thus necessary to provide, at the software level, an automatic means to convert data captured from a motion capture systems to the Stimulator.

In terms of mechanics, the device chassis and all the parts in contact with the body need to be implemented in a bio-compatible material. Moreover, since a joint operation with ultrasound can be required, the main handle of the device, that is, the part that needs to be positioned around the subject, needs to be small enough not to hinder the Ultrasound device

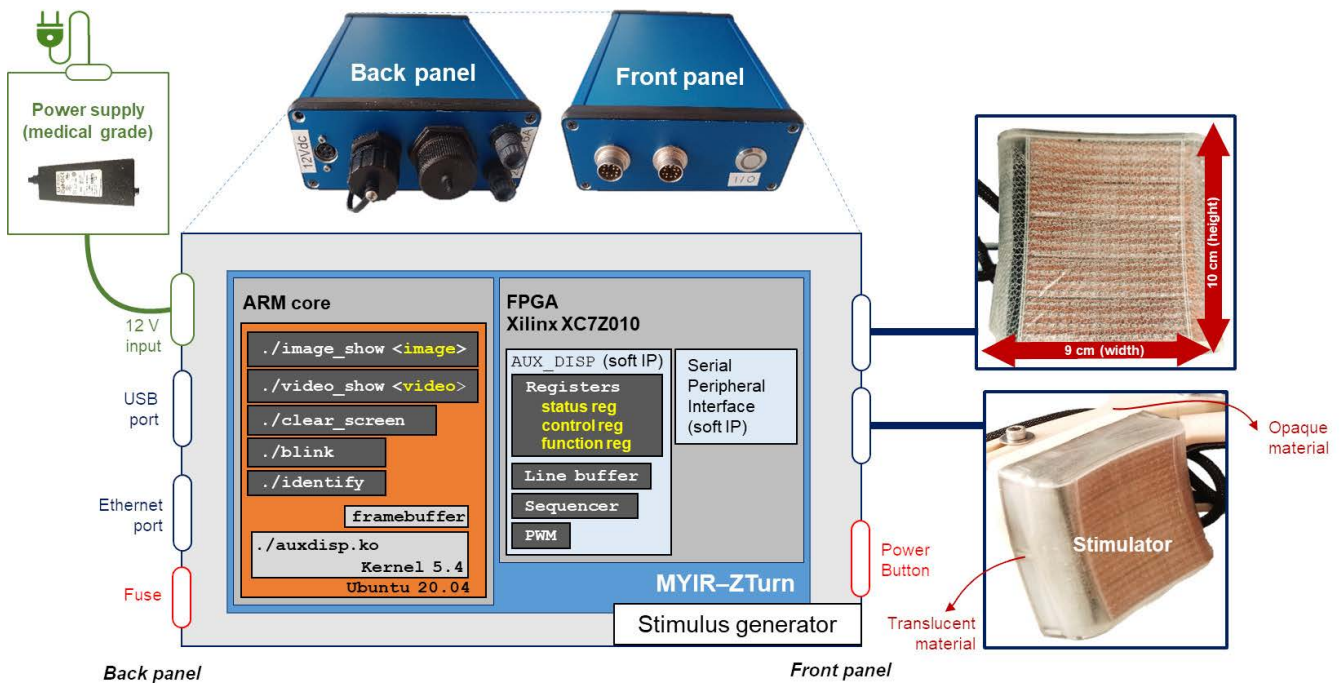


FIGURE 2. Back panel of the TCFVS system and the front panel with peripherals and interfaces with detailed TCFVS block diagram and operation scheme such runs using the defined functions executed on FPGA ARM core.

movements. A mechanical holder to host the displays with a predisposition to integrate an Ultrasound probe is then an optional requirement, and it is necessary to design mechanics to guarantee the arbitrary positioning of the display around a women's womb.

The next subsection deals with the design of the hardware and the associated software of the device. The pattern generation algorithm that is fundamental to provide full integration with inertial measurements is detailed instead in Sec. III.

B. DESIGN

Fig. 2 shows a block diagram of the TCFVS comprising the following parts: power supply, stimulus generator (main module), and the stimulator (i.e., the *display*, overall two). Our solution is a double LED matrix controlled using an AC-powered control unit, interfaced with a personal computer, carefully engineered from the mechanical viewpoint to meet the above requirements.

First and foremost, a medical-grade power supply is used in TCFVS to power up the entire system, which complies with the International Electro-Technical Commission (IEC) 60601 safety and protection standards. The Stimulus generator includes an MYIR-ZTurn board, power connectors, and communication protocols in a small-size ($16 \times 12 \times 5.1 \text{ cm}^3$) box to increase connectivity and portability. An external connector for power supply, a fuse, a Universal Serial Bus (USB) port, and an Ethernet port are mounted in the Back panel. On the other side of the box, the Front panel comprises the display connectors and a power button.

In the following subsections, we will discuss each building block of the TCFVS.

1) STIMULATOR

The Stimulator in Fig. 2 sends visual stimuli to the fetuses. The body of this Stimulator (Width = 9 cm and Height = 10 cm) includes two enclosures to provide a firm grip and protect electronics. These two enclosures are rapid prototyped with different materials for optimal light characteristics (e.g., translucent and opaque). The material used in the first enclosure is bio-compatible to assist skin usage (Stratasys Biocompatible MED610 [6]), and this material is translucent to disperse light through it. Besides, the enclosure is fabricated onto the shape of a parabola (i.e., in the shape of a mother's womb) to disperse light directly onto the skin. Indeed, the enclosure has a double curvature on its horizontal and vertical facets. The horizontal facet has a continuous arc (the flexible PCB supports this bend), and the vertical facet has a five-segmented arc to enable the placement of each LED driver on the tangent of each segmented arc. The radius of these arcs is an average measure of the pregnant women's abdomen in their third trimester. This parameter that has been refined and finalized in the final prototype based on a first user experience with a mock-up. The other enclosure offers support and provides a room for electronics. The material used in the second enclosure is a Stratasys ULTEM 9085 [7] – a hard Opaque material. Previous studies illustrate the importance and the need for a red light near 650 nm wavelength (farthest light in the visible spectrum) in fetal

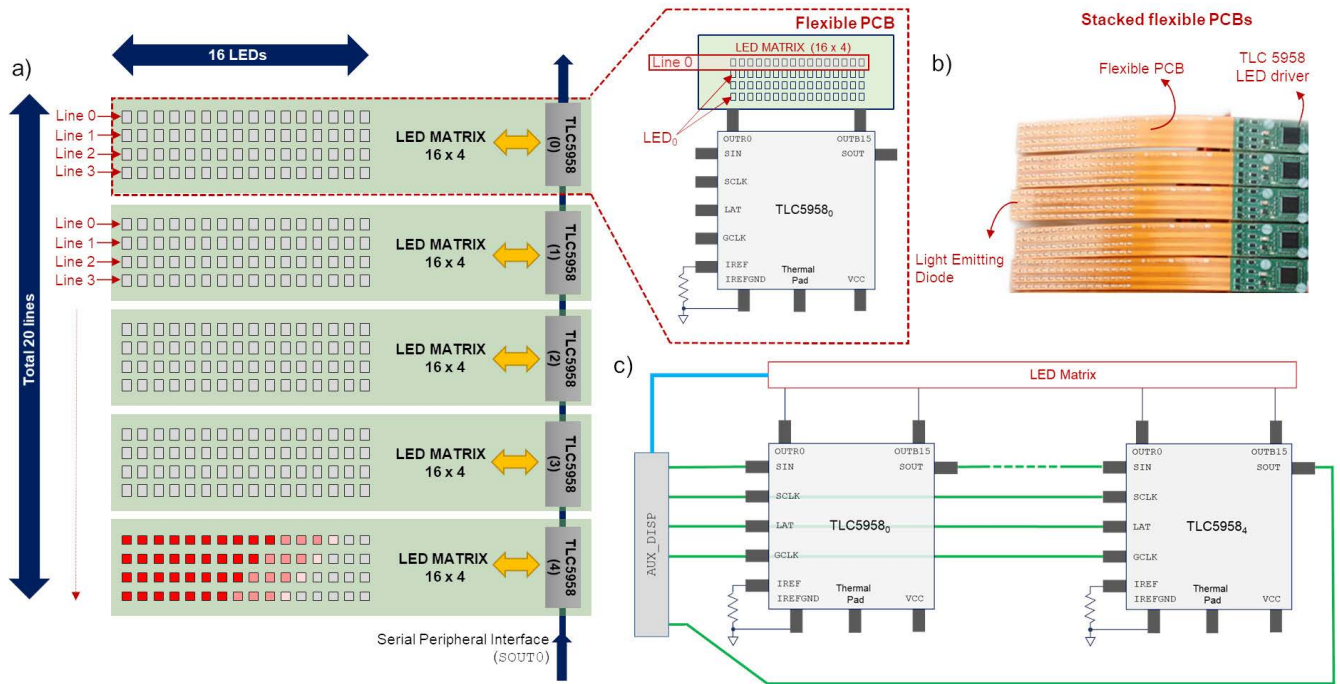


FIGURE 3. a) Schematic representation of the stimulator comprising vertically stacked flexible Printed Circuit Board (PCB), overall 20 lines of an 16 LED array. Inset TLC5958 is connected to every four lines of the 20 line display for a systematic control of LEDs. b) Stacked PCBs inside the Stimulator and c) TLC5958 serially interfaced to AUX_DISP.

visual stimulation experiments [8]. The chromophores in the human skin scatter this red light to reduce its energy density with increasing skin depth [9].

For multi-array displays, Light Emitting Diodes (LED) are highly efficient and available in smaller form factors to be preferred as the light sources, especially in medical applications [10], [11]. LEDs, indeed, provide high reliability, acute light control, faster switching cycles, and longer lifetimes [10]. Considering these facts, in TCFVS, the Stimulator comprises 320 LEDs (King-bright, wavelength 640 nm, power 84 mW, and geometry 1.6 mm × 0.8 mm [12]) organized in 20 rows.

Fig. 3a shows every single row on the Stimulator that has 16 LED, and the resolution of the Stimulator is then 16 × 20 pixels. With such a large number of LEDs, a dedicated driver is necessary to enable the concurrent operations of many rows. In this system, we have used the TLC5958, which enables the grouping of multiple rows [13]. Four rows of the Stimulator (i.e., 4 × 16 LED) are grouped into one TLC5958.

For illustration purposes, Fig. 3a shows each row in every TLC5958 named as Line 0, Line 1 ... Line 4. The TLC5958, moreover, is a 48 channel constant current LED driver that supports flexible multiplexing and a high refresh rate. For ease of understanding, Tab. 1 shows the TLC5958 pin description. The inset of Fig. 3a shows how a LED_x of any row is connected to OUTR_x in the TLC5958. For instance, LED₀ of Line 0 is connected to OUTR₀, and LED₁ of Line 0 is connected to OUTR₁. This way, every LED in the multi-array display is systematically connected

TABLE 1. TLC5958 pin description.

Pin	Direction	Description
GCLK	I	Grayscale Clock
GND	-	Ground
IREF	-	Maximum Current
IREFGND	-	Current Ground
LAT	I	Latches the data either for GrayScale Control or for Function Control Register
OUTX0-X15	O	Constant Current Output for Red, Green and Blue LEDs. (X = R or G or B)
SCLK	I	Serial Data Shift Clock
SIN	I	Serial Data Input
SOUT	O	Serial Data Output
VCC	-	Power Supply

to TLC5958. This logical connection is physically achieved using a multi-layer flexible Printed Circuit Board (PCB). One display comprises five PCBs (each one having 64 LED) that are stacked one upon each other to constitute a Stimulator (see Fig. 3b). Fig. 3c shows how the five TLC5958 are serially connected (i.e., TLC5958₀, TLC5958₁, ..., TLC5958₄) for effective scheduling and communication. Further, each Stimulator (one per display) is connected to the stimulus controller using serial connectors.

2) STIMULUS GENERATOR

The Stimulus Generator is implemented using a low-cost MYIR-ZTurn previously depicted in Fig. 2. It is a high-performance System on Chip (SoC) built around the Xilinx (XC7Z010) [14] that includes an ARM Core (Cortex-A9 Processor as a host CPU), and Xilinx 7-series

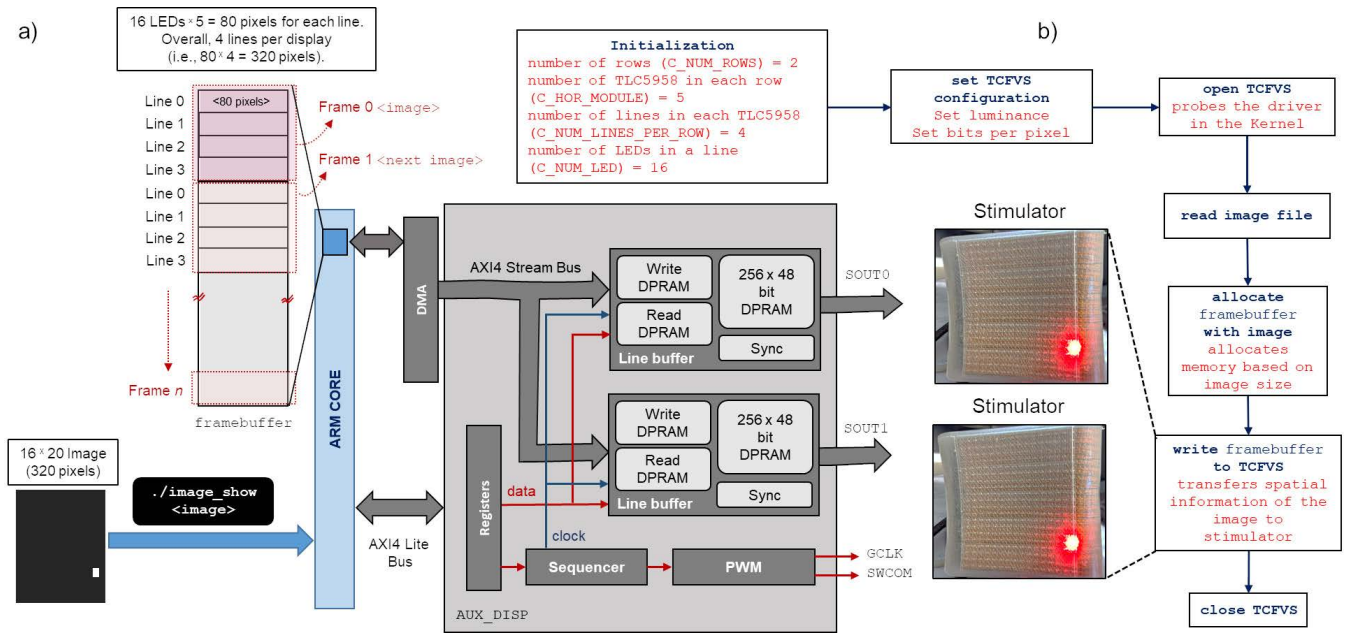


FIGURE 4. a) AUX_DISP implementation on FPGA to control FPGA using registers. b) Sequence to work synchronously and streamline the frame rendering on the Stimulator.

Field Programmable Gate Array (FPGA). This SoC provides significant support, flexibility, and simplicity towards hardware implementation. These important points, *inter alia*, have always paved the way to several intense applications in medicine, aerospace, and military applications. Moreover, the SoC allows users to install Linux on its ARM core, thus providing general-purpose software capability to run sophisticated algorithms. In summary, MYIR-ZTurn provides flexible support to achieve a successful outcome in our Stimulator design for hardware-software co-integration.

We have interfaced the Stimulator directly to AUX_DISP, a software Intellectual Property (soft IP) synthesized in the MYIR-ZTurn FPGA using the XILINX Vivado software [15]. AUX_DISP has been designed to support sixteen TLC5958 devices (i.e., the multiple LED drivers). In the FPGA, AUX_DISP includes Registers, Line buffer, Sequencer, and a Pulse Width Modulation module PWM, to schedule the static images at distinct times to yield high refresh rates (see Fig. 4). The Registers initialize, control, and coordinate the display operation cycles. Practically, the Line buffer queues the pixels from the framebuffer onto a Dual Port Random Access Memory (DPRAM) with a size of 256×48 bit (to support sixteen TLC5958 devices). The operation of the framebuffer will be illustrated in much detail in the next section. In each display, we have used five TLC5958 to obtain 5×16 LED, i.e., 80 pixels per four lines (overall 320 pixels per display, organized in four blocks). In fact, these four lines of 80 pixels just require a size of 80×48 bit across the DPRAM. The Sync feature in the Line buffer synchronizes the cross clock domain mismatch in the AUX_DISP for providing a smooth data

transfer within the system. The Sequencer coordinates all the components in AUX_DISP by regulating the device clock for effective operation. The PWM unit regulates the overall device brightness to have a uniform light intensity across all LEDs (which is set by the user through the dedicated Registers). In practice, the Line Buffer is a sophisticated shift register that specifically shifts the framebuffer content onto the Stimulator at each clock cycle. For faster data communication between the host CPU and the AUX_DISP, we have instantiated two different ARM AMBA buses (for more detail, see [16]). The first, the AXI4 stream bus transfers high-speed data streaming at 100 MHz between the framebuffer and the Line buffer. To offload the main ARM CPU, this transfer is assigned to a Direct Memory Access (DMA) for a continuous data/address transfer. The second AXI lite bus uses low throughput memory-mapped communication to control or read the TCFVS system status from the host CPU.

Fig. 4a shows the complete data flow in the AUX_DISP of the FPGA controlled by the ARM core. The corresponding Linux drivers for the AUX_DISP module were written and automatically probed (`modprobe`) at the Kernel start-up. In our design, the ARM core of the MYIR-ZTurn runs Ubuntu Linux 20.04, with Kernel 5.4. At start-up, during Linux initialization, the software also defines the physical pins of AUX_DISP to be used at FPGA-level, its low-level configuration, and driver properties to access the hardware and pose a smooth execution of the device during stimulation rendering (see Fig. 4b). The framebuffer is a memory allocation (similar to a queue) in the ARM Core, where the image before execution is stored, as exemplified in Fig. 4a. Any image in

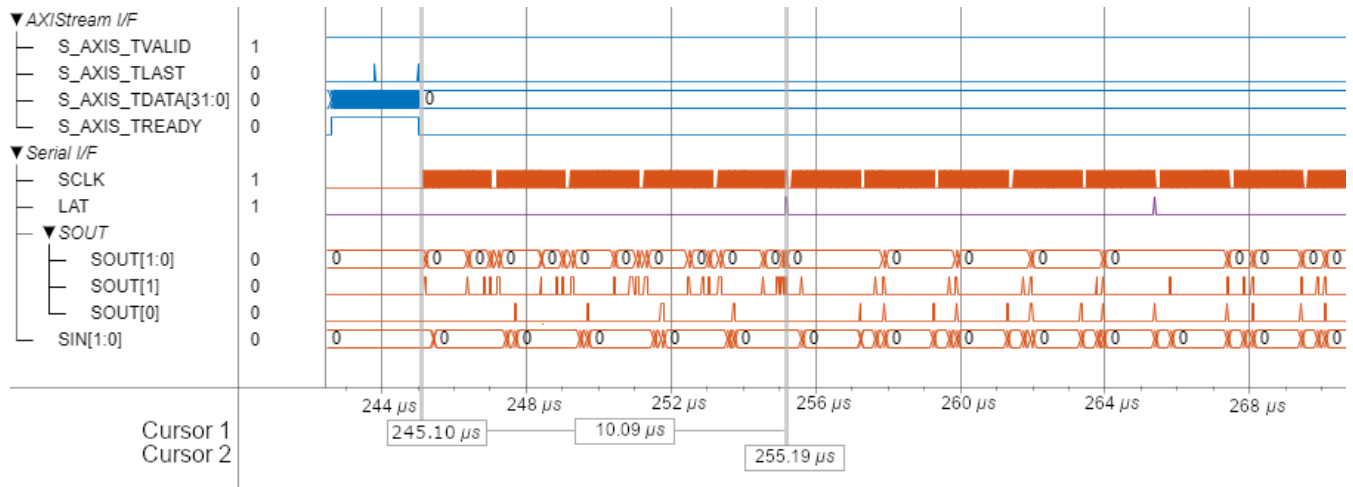


FIGURE 5. Timing diagram of AUX_DISP (FPGA implementation).

TABLE 2. Xilinx XC7Z010 FPGA resource utilization (XILINX).

Resource	Utilization	Available	Utilization %
LUTs	4623	53200	8.69
LUT RAM	647	17400	3.72
FF	5650	106400	5.31
BRAM	3	140	2.14
IO	18	125	14.40
BUFG	6	32	18.75
MMCM	1	4	25.00

the framebuffer is memorized in a format that can be directly rendered onto the Stimulator as a visual stimulus without other modifications. The framebuffer can be used to store either an image or a sequence of images (i.e., a video). TCFVS supports 48 bpp (bits per pixel) grayscale images only. If an image or frame with a lower bit per pixel (e.g., 16/24/32 bpp) needs to be used as stimulation, TCFVS automatically pads the remaining bits to zero using the (Set bits per pixel feature schematized in Fig. 4b).

Fig. 5 shows the input and output vectors of the AUX_DISP implemented on the FPGA. The figure shows the AXIStream I/f group, i.e., the input vector indicates the AXI4 Stream Bus (S_AXIS_TREADY, S_AXIS_TDATA, S_AXIS_TLAST, and S_AXIS_TVALID), that is, the high-speed data streaming between the framebuffer, and the Line buffer. Here, the S_AXIS_TLAST indicates the end of the data-stream, for instance, Line 0 has (80 × 48 bit) data in the framebuffer is transferred to the DPRAM inside the Line buffer using S_AXIS_TDATA and S_AXIS_TREADY.

Next, the FPGA needs to offload the received data to the TLC5958s. We already know that TCFVS has two displays (C_NUM_ROWS = 2), each display consists five TLC5958 (C_HOR_MODULE = 5). The AUX_DISP offloads the data through LAT, SCLK, and SOUT connected TLC5958 (see Tab. 1). Here, in Fig. 5, the LAT indicates the transfer of five pixels to the TLC5958s, that is, LED₀ in Line 0 of

every TLC5958 has received the data (see Fig. 3). Similarly, all the LEDs connected to their corresponding lines across the display (320 pixels) receive the data from the AUX_DISP sequentially. Each LAT after every “five” pixels has been latched out through SOUT in 10 μs (see Fig. 5 from Cursor 1 at 245 μs to Cursor 2 at 255 μs). The AUX_DISP takes 660 μs, approximately to display a single frame as a stimulus to the Stimulator, which means the AUX_DISP support higher refresh rates until 1500 Hz. Such high refresh rates are meaningless for our application (they are not relevant for the fetal eye), hence, the TCFVS serial clock is fine-tuned to provide refresh rates until 250 Hz. Tab. 2 shows the summary of the detailed resources and utilization for the custom FPGA hardware of our TCFVS device, here, the parameters are LUTs (Lookup Tables), LUT RAM (Lookup Table Random Access Memory), FF (Flip Flop), BRAM (Block Random Access Memory), IO (Input Output), BUFG (Global Buffer), and MMCM (Mixed Mode Clock Manager). The utilization summary involves both the ARM Core and the AUX_DISP implementations in the FPGA.

Tab. 3 shows the TCFVS commands useful to display generic patterns onto the Stimulator or to perform display reset and detect other configuration parameters. Device commands are specific program functions in the TCFVS that automatically invoke the Kernel module and configure Stimulator parameters, such as lines, the number of TLC5958 used, the color depth of the image, and so on. Further, the program sets the brightness control in the configured TLC5958 for a uniform light distribution (all equal LED current per pixel) hence providing an adequate luminance. At this point, the ARM core, which needs to process a static image of a particular sequence, can allocate memory to fill the framebuffer size using the DMA. Finally, a write command transfers the framebuffer image to the physical stimulator (see the internal photo in Fig. 4b).

To be directly rendered onto the Stimulator, images always need to be converted so that they match its internal hardware scheme. The sequencer in the Line buffer

TABLE 3. Main TCFVS commands.

Command	Description	Parameters
Stimulus execution commands		
<code>./image_show <image></code>	Sets a file <image> in Stimulator	<image>: Characters {A...Z, 0...9}
<code>./video_show <video><repeat></code>	Runs a file <video> for <repeat> times	<video>: Characters {A...Z, 0...9} <repeat>: Numbers {0-9}
<code>./blink <time></code>	Blinks a 4 × 4 dot for a given <time>	<time>: Numbers {0...9}
Device control commands		
<code>./init_connection</code>	Initiates connection, provides device status, and tests the Stimulator	–
<code>./clear_screen</code>	Clears the Stimulator screen	–
<code>./identify</code>	Identifies the Stimulator displays	–
<code>./emergency_stop</code>	Stops TCFVS for emergency	–
<code>./device_stop</code>	Stops the current stimulation execution	–
<code>./device_info</code>	Provides the IP address information of the device	–
<code>./device_shutdown</code>	Safely shuts down the device	–

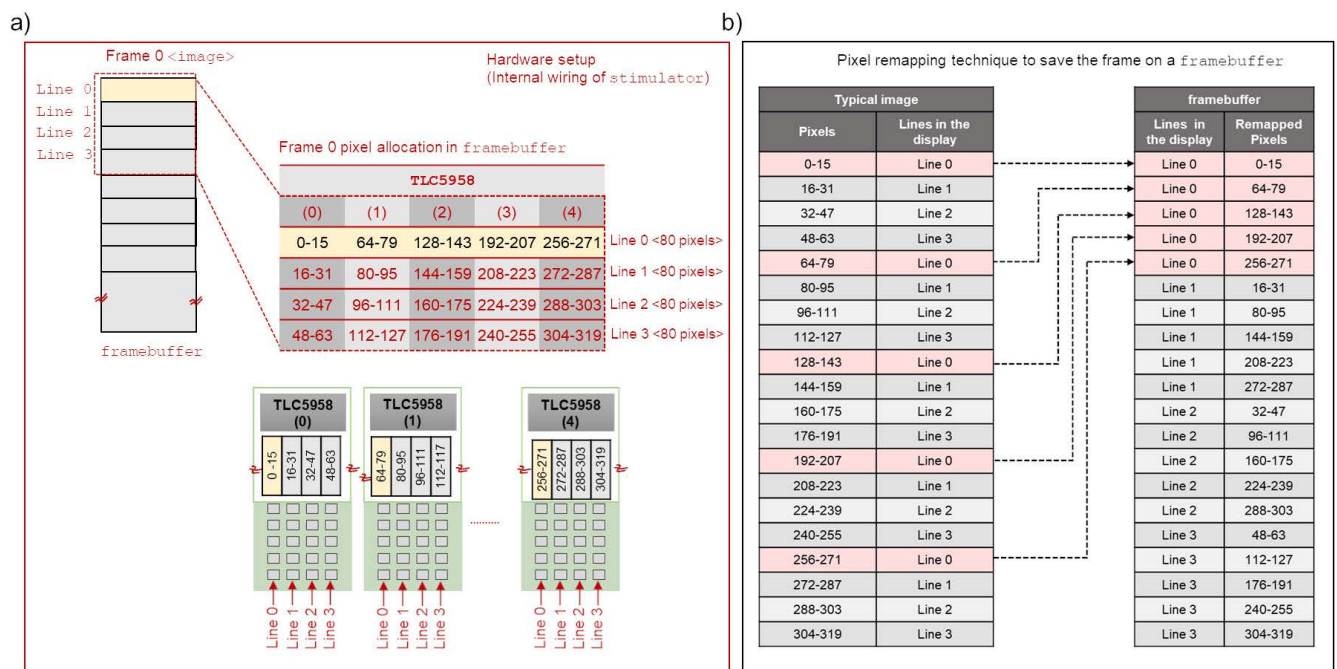


FIGURE 6. a) Internal wiring sequence of the Stimulator that illustrates how pixels are stored and retrieved in the framebuffer to render visual stimulus. b) Pixel remapping technique that remaps an image according to the framebuffer specifications, to have an accurate stimulus.

runs in the following order: (i) it reads the Line X from the framebuffer, (ii) it updates the DPRAM in the Line buffer, and (iii) it transfers the data in Line X in all TLC5958. Compared to a sequential line rendering (one by one), this execution mode is efficient and fast to render the static image onto the Stimulator because it transfers four lines at a time concurrently. Fig. 6a shows how the framebuffer is associated with the TLC5958. The organization of the framebuffer is such as an image remapping technique is mandatory to display images correctly.

Fig. 6b graphically shows the remapping process that replaces every pixel in the static image (organized as shown later in Fig. 7) to maintain the previously described relationship of the image concerning the

framebuffer organization. Eventually, the loop iterates $C_HOR_MODULE \times C_NUM_LED$ times so that all effective pixels in the line are sequentially copied (using the built-in function `memcpy`) to the framebuffer. The loop iterates for 80 effective pixels of every single line that constitutes the Stimulator resolution (320 pixels overall, i.e., 80×4). This pixel remapping hardware implementation was conscientiously planned to enable debugging during execution, such as detecting hardware failure, checking frame rate, and getting operational feedback on each LED line. The inset of Fig. 7 shows the example <image> and its remapped version in the framebuffer. When the device commands are invoked, the system automatically reads the static image onto the framebuffer and renders it as a stimulus on the Stimulator.

```

#define C_NUM_LED          16 // Number of LED's in a line in one TLC5958
#define C_HOR_MODULE      5 // Number of TLC5958 in the display
#define C_NUM_ROWS        2 // Number of display
#define C_NUM_LINES_PER_ROW 4 // Number of lines connected to each TLC5958
#define C_SIZE_LINE       C_NUM_LED*C_HOR_MODULE // Number of pixels in a line
//for e.g., Line 0 has 16 * 5 = 80 pixels
#define C_DISPLAY_1       C_NUM_LED*C_HOR_MODULE*C_NUM_LINES_PER_ROW // Number
//of pixels in a display for e.g. Left display has 16(LEDs)*5*4(lines) = 320 pixels

// Image remapping
for (y = 0; y<C_HOR_MODULE; y++){
  for (x=0; x<C_NUM_LED; x++){
    memcpy (framebuffer + (x + C_NUM_LED * y + 0*C_SIZE_LINE), image + x + 64 * (y)  0 * C_NUM_LED, sizeof(pixel_t)); // Line 0 Display 0
    memcpy (framebuffer + (x + C_NUM_LED * y + 1*C_SIZE_LINE), image + x + 64 * (y) + 1 * C_NUM_LED, sizeof(pixel_t)); // Line 1 Display 0
    memcpy (framebuffer + (x + C_NUM_LED * y + 2*C_SIZE_LINE), image + x + 64 * (y) + 2 * C_NUM_LED, sizeof(pixel_t)); // Line 2 Display 0
    memcpy (framebuffer + (x + C_NUM_LED * y + 3*C_SIZE_LINE), image + x + 64 * (y) + 3 * C_NUM_LED, sizeof(pixel_t)); // Line 3 Display 0
    memcpy (framebuffer + (x + C_NUM_LED * y + C_DISPLAY_1 + 0*C_SIZE_LINE), image + x + C_DISPLAY_1 + 64 * (y) + 0 * C_NUM_LED, sizeof(pixel_t)); // Line 0 Display 1
    memcpy (framebuffer + (x + C_NUM_LED * y + C_DISPLAY_1 + 1*C_SIZE_LINE), image + x + C_DISPLAY_1 + 64 * (y) + 1 * C_NUM_LED, sizeof(pixel_t)); // Line 1 Display 1
    memcpy (framebuffer + (x + C_NUM_LED * y + C_DISPLAY_1 + 2*C_SIZE_LINE), image + x + C_DISPLAY_1 + 64 * (y) + 2 * C_NUM_LED, sizeof(pixel_t)); // Line 2 Display 1
    memcpy (framebuffer + (x + C_NUM_LED * y + C_DISPLAY_1 + 3*C_SIZE_LINE), image + x + C_DISPLAY_1 + 64 * (y) + 3 * C_NUM_LED, sizeof(pixel_t)); // Line 3 Display 1
  }
}
write(tcfvfs, framebuffer, C_NUM_ROWS * C_NUM_LINES_PER_ROW * C_SIZE_LINE * sizeof(uint48_t)); // write the remapped image to the TCFVS for display

```

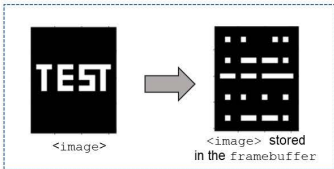


FIGURE 7. A snippet of the C program that uses the built-in memcpy function to copy the image onto the framebuffer using our pixel remapping technique (detailed next). (Inset) A sample image after being remapped using our pixel remapping technique, ready for rendering.

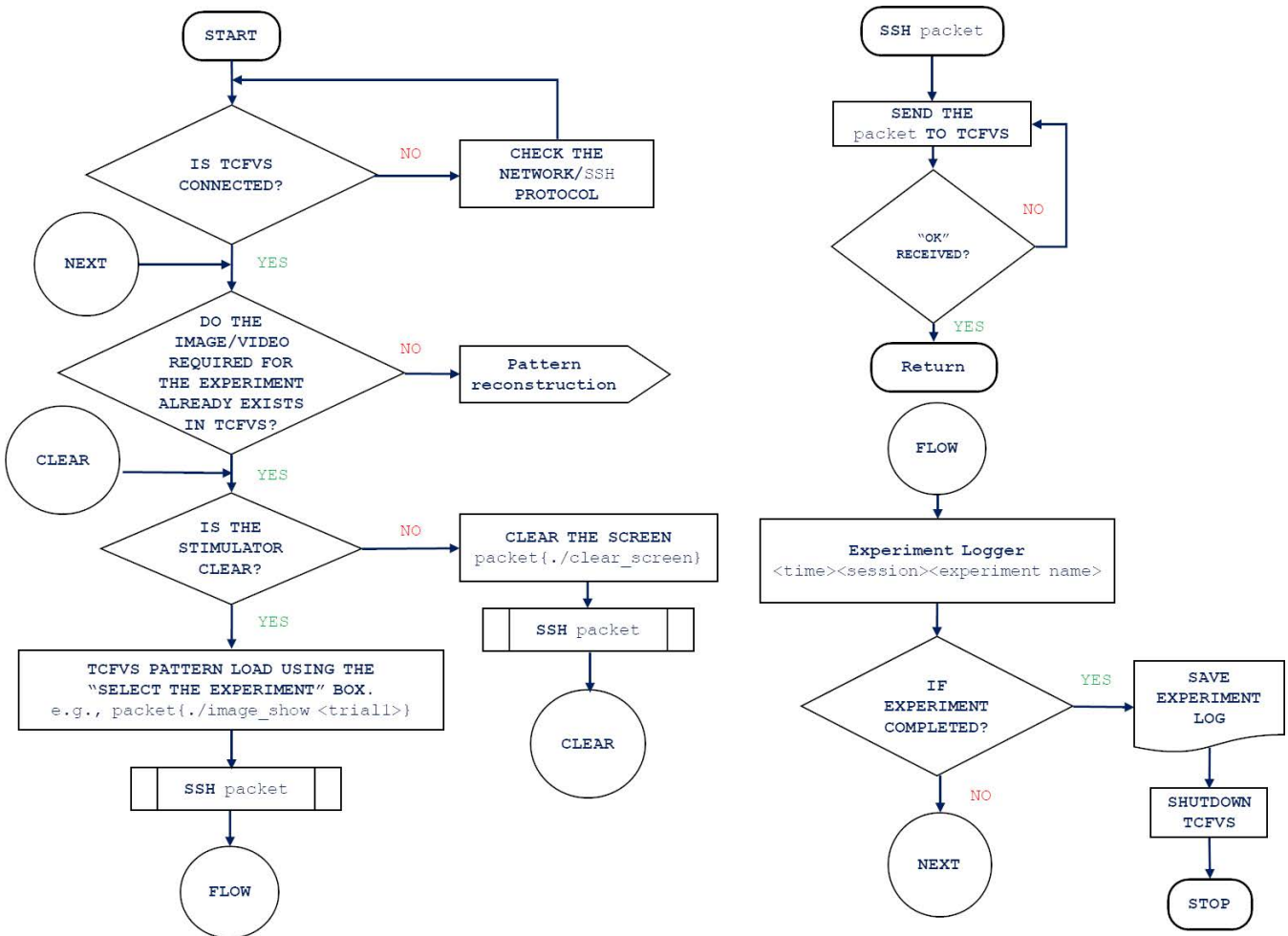


FIGURE 8. Flowchart of the system programming.

3) HARDWARE AND SOFTWARE TOOLCHAIN

We have written high-level software that calls low-level sequences of device commands for a seamless operation. This software allows the experimenter to configure and run an experiment and monitor the device status.

Fig. 8 shows the system software’s functional flowchart. TCFVS uses a timed network connection for communication with a Personal Computer (PC) that connects to the

device using a Secured Shell Host (SSH). Eventually, every connection/communication with the device and the host PC provides prompt feedback on its error or system status as a notification to the experimenter. In particular, the Check the Network/SSH protocol feature provides error messages in the case of connection failure and provides methods to establish a connection. Afterward, the PC handshakes with the device using the low-level Device control

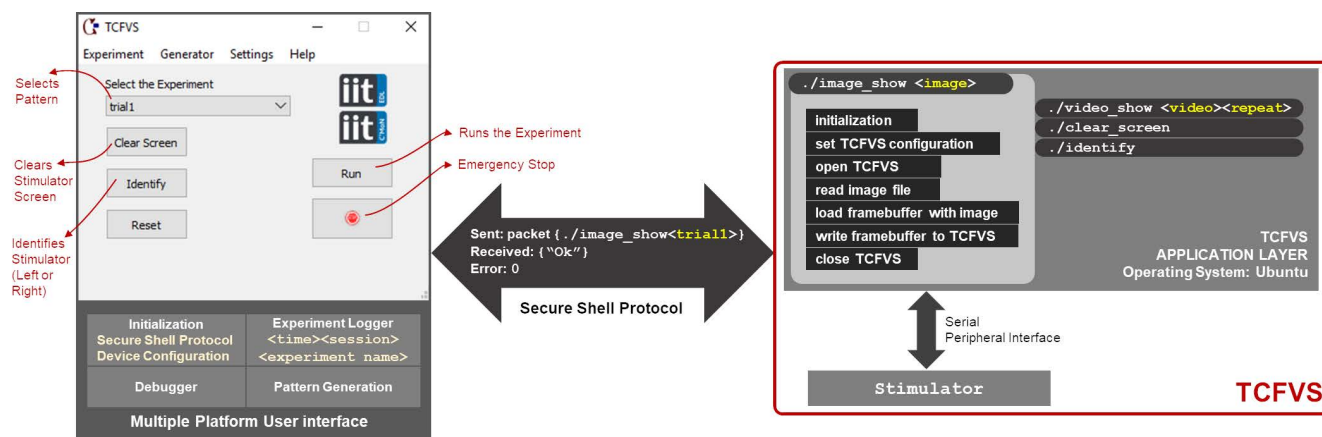


FIGURE 9. (Left) User Interface on the Personal Computer, where the experimenter can choose the stimulus and apply execution to render the stimulus on the displays. (Right) Low-level internal commands that are called by the User Interface.

commands in Tab. 3., that also enlists the accessible stimuli available in the device to the experimenter. For visual stimulus rendering, the experimenter, can load the stimulus from these accessible set using `Select the experiment` box in the UI (see Fig. 9). Otherwise, the experimenter can create a pattern using the `Pattern reconstruction` tool (illustrated in detail in the following sections) and transfer it to the device. In the `Stimulator`, clearing the screen is a necessary step before presenting a new stimulus, therefore, the software checks if the display is clear, and if not automatically invokes the clear screen process before the stimulus rendering. After the stimulus rendering, the experimenter can use these example methods to repeat the experiment with another stimulus or terminate it. On a terminate event, the event logger monitors the `time`, `session`, and `experiment name` during the experiment, saves them as a log, and finally shuts down the device.

Fig. 9 shows the TCFVS User Interface (UI). The combination of Python 3.7, and Qt 5.2 (a cross-platform software development framework that can run in various hardware and operating systems platforms such as Windows, Macintosh, and Linux) enabled us to develop a Multiple platform User Interface to perform the fetal visual stimulation experiments, without having any need to change the code across multiple operating systems and retaining the same execution speed and native built-in drivers. The UI was designed to be functional and straight forward, from the user perspective. Moreover, it has been designed to comply with the functional flowchart given in Fig. 8. The primary function of the UI is to provide the stimulation data for TCFVS execution and continuous monitoring in both time-domain and a data log space. Our UI enables the user to program an experiment with all necessary operations for its set-up.

The UI enables the user to change the TCFVS connection parameters. In these cases, the experimenter needs to enter the information in a “Settings” window to establish a connection with the device. Using the UI, an experimenter can choose any stimulation file to perform or plan any experiment

and observe the fetal reactions using an Ultrasound system. After the selection, the UI automatically sends the required low-level commands to the TCFVS using SSH to execute the corresponding complex high-level actions. In the case of further customizing, the user can automate or edit the experiment sequence using the Command Line Interface (CLI). This scripting feature allows the experimenter to run any stimulus sequence (video) for a prolonged period or set the `Stimulator` to a static image. In addition, the UI monitors and records a series of metadata, i.e., `session` information, `experiment name`, and `perform time-stamp` for any executed experiment. These data can be useful for successive post-processing and data analysis.

III. STIMULUS GENERATION AND PATTERN RECONSTRUCTION ALGORITHM

Stimulus generation is a fundamental process to enable the effective rendering of stimulation files on the `Stimulator`. TCFVS can render simple geometric shapes (e.g., circles, squares, diamonds) and figures, as well all create motion patterns with a max refresh rate of 250 Hz. Owing to a Capture toolbox, TCFVS can render not only constant velocity motion patterns but also biological motion patterns. For biological motion generation, the experimenter can use any motion capture system. As a first demonstration, we used `ViconTM` [17] to record grasping movements by human adults (see Fig. 10a).

The `Vicon` coordinates were then to `Pattern coordinates` in the formats of portable network graphics (PNG) or animated audio-video interleaved (AVI) using `Real-Time Motion Capture Toolbox` in `MatlabTM` [18]. In this work, we have used a resolution of 400×500 pixels, therefore at multiples of the `Stimulator` aspect ratio (16×20 pixels). Further, we have set the `Capture toolbox` to capture frames at 17.5 fps. For both static images and videos, this toolbox output data includes the high-resolution movement of the `Pattern coordinates` by solid white circles on a black screen. Observe that the algorithm presented in this work does not lose generality when the kinematic

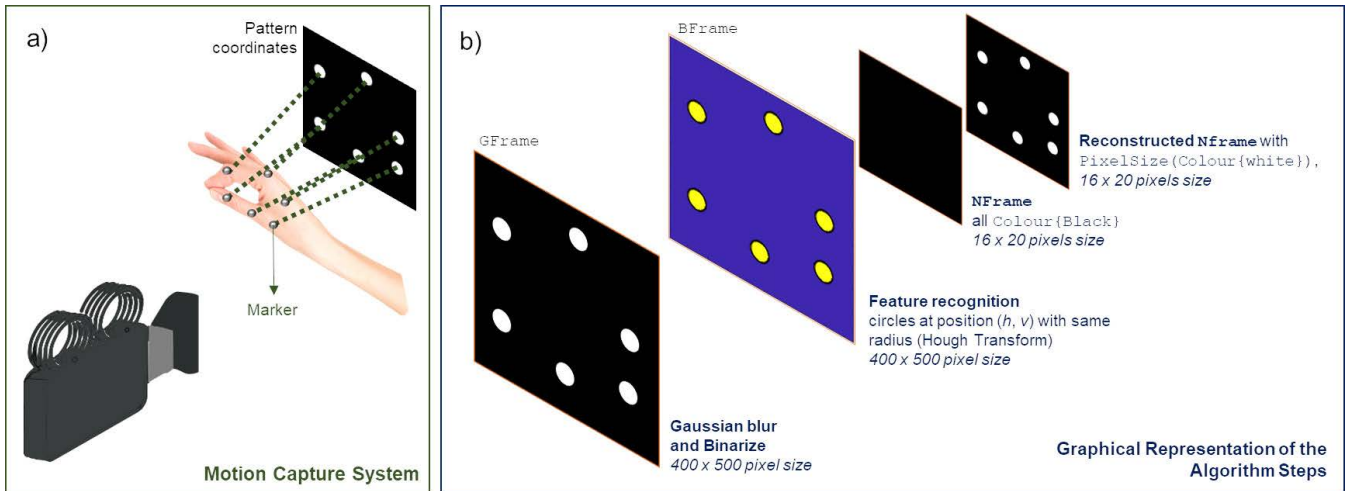


FIGURE 10. a) An example of a motion capture system that precisely captures the markers fixed on the human wrist with a pattern acquired by the cameras. The solid white circles in the image behind the wrist show the captured marker's position. b) Image reconstruction of $Frame$ to $NFrame$ so that it can be correctly rendered on TCFVS.

information is converted to a different resolution, even when it is not a multiple of the Stimulator aspect ratio.

The physical size of the Stimulator is 16×20 for a single display and 32×20 for two displays. This resolution does not match with the stimulation file, therefore, the data has to be resized to fit the TCFVS display. Down-scaling techniques can be used to resize an image to a suitable size, thus providing significant capabilities in several applications, for instance, microscopy, remote sensing, soil moisture mapping, and so on [19]–[21]. However, these algorithms result in information loss and surely, in our context, can alter the `Pattern coordinates` [22]. An alternative option is to modify the above-mentioned conventional techniques to match our requirements. However, this is far to be considered feasible for realization: mostly, these algorithms and their resulting adaptation to our context result in any case in an information loss that introduces random noise and impacts the movement of solid circles. This loss does not preserve accuracy in the movements, which is fundamental for scientific exploration. Movements, indeed, shall be rendered as natural as possible. To resolve this issue, we have created an algorithm, which reconstructs the `Pattern coordinates` to a suitable format to support our system display. In our algorithm, one or more pixels can be selected to increase or decrease the brightness, that is, the size of the pattern is adjusted to any required pixel size. This way, pixel size is directly related to the control of the brightness of the Stimulator (more pixels typically indicate higher brightness).

Alg. 1 describes the implementation of our image reconstruction technique that runs in a PC connected to the device. Essentially, the output data with `Pattern coordinates` (see Fig. 10a) from the toolbox has to be free from noise for processing, so that it only contains clear patterns for processing. We have implemented the state-of-the-art algorithms `GaussianBlur` and `Binarize`, as stand-alone functions

Algorithm 1 Pattern Reconstruction (PIXSIZE Is Generic)

```

Frame ← motionData;
PixelSize = PIXSIZE;
AspectRatio = 16/20;
resizeFactor = Frame/AspectRatio;
while I = no_of_frames do
    GFrame ← GaussianBlur (Frame);
    BFrame ← Binarize (GFrame);
    Z ← HoughTransform (BFrame);
    Z ← Z/resizeFactor;
    NFrame (AspectRatio) = Color.Black;
    while N = length (Z) do
        NFrame ← PixelSize (Color.White);
        N ← N-1;
    end while
    TFrame[I] = NFrame;
    I ← I-1;
end while

```

in our toolchain to achieve this noise filtering (`GFrame` and `BFrame` outputs, respectively). `GaussianBlur` smooths the frame, hence subsequently reducing the high-frequency noise. `Binarize`, instead, suppresses each pixel color to two-level `Color.Black` or `Color.White` to form the `BFrame` given in Fig. 10b.

The Hough transform, a technique used to extract locations and orientations of basic shapes from any given binarized image [23], is used here to precisely identify each pattern (here, named as x) in `GFrame`, so that each of them can be collectively identified as $x \in \mathbb{Z}$ (for instance, the example of Fig. 10b contains six patterns in \mathbb{Z}). At this point, the Hough transform can precisely evaluate the edges or lines in the `GFrame`, and map the central position of the `Pattern coordinates` (with h – horizontal position and v – vertical position) and size of the feature (here identified as r) to x ,

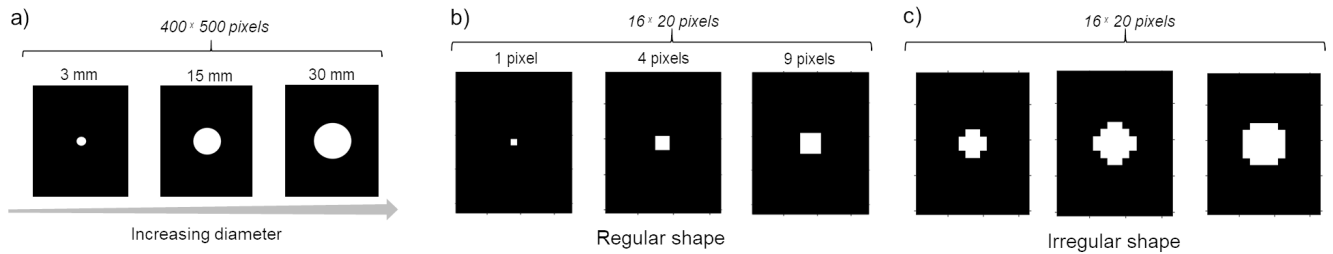


FIGURE 11. a) Sample data that represents high-resolution data output from pattern coordinates. b) Re-scaled outputs having a regular shape. c) Re-scaled outputs with deformed shape that are not suitable for the use as stimuli in the Stimulator.

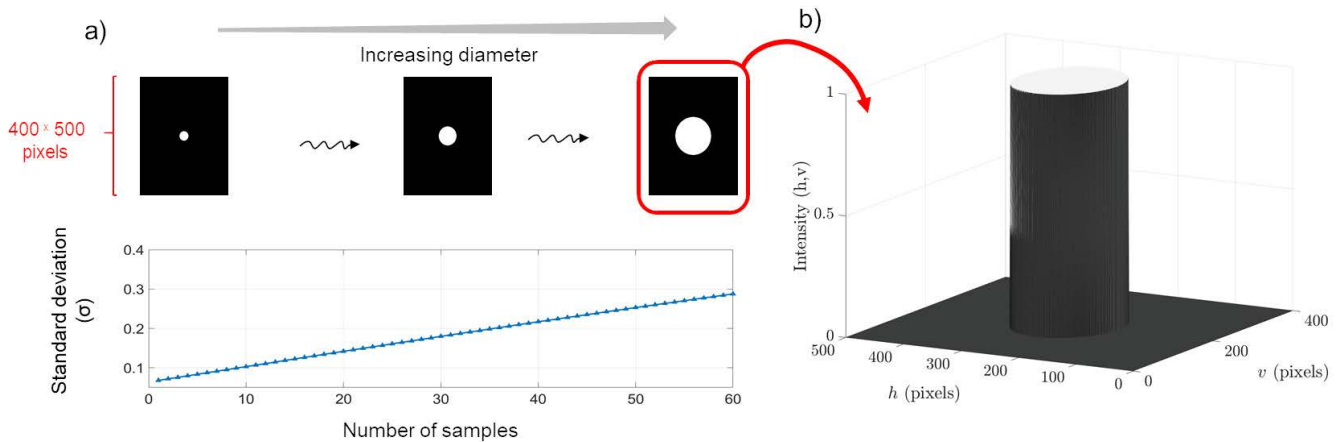


FIGURE 12. a) Diameter of the solid circle that gradually increases to show subsequent increase in standard deviation of an image. b) Three dimensional view of the sample image that represents a pattern coordinates of higher dimension.

where $x = \{h, v, r\}$ (that is, the yellow patterns in `BFrame`). The orientation and size of the patterns in \mathbb{Z} are referred to `BFrame`, therefore, for effective image reconstruction, they are resized by a `(resizeFactor)`. Further, the resized patterns in \mathbb{Z} are used for image reconstruction: the `NFrame`, an image of the `Stimulator` is initialized with black pixels (identified as p). Meanwhile, the pattern reconstruction algorithm runs for every pixel in the `NFrame`, and subsequently replaces p with `Color.White`, if p belongs to \mathbb{Z} , as shown in Eqn. 1,

$$f(p) = \begin{cases} \text{Color.White,} & \text{if } p \in \mathbb{Z} \\ \text{Color.Black,} & \text{if } p \notin \mathbb{Z}. \end{cases} \quad (1)$$

Likewise, the image reconstruction algorithm performs the above actions on every other pattern in \mathbb{Z} . This way, the patterns in the `NFrame` have the same spatial characteristics of the `Pattern` coordinates in the output data from the toolbox. At this point, the reconstructed `NFrame` readily supports our TCFVS hardware. In the case of a series of images, Alg. 1 runs through every frame to compile a stimulation video that has no artifacts nor noise errors.

IV. ALGORITHM VALIDATION AND FIRST MEASUREMENT RESULTS

First, we present the downscaling algorithm validation that has been achieved using a custom test set-up that we will discuss here. Second, we will show some first tests on the

field with the device before systematic research that will be part of other works.

Each `Marker` can be placed on any body part or limb to capture any mechanical movements. Fig. 11a shows an example of sample images to identify the possible `Pattern` coordinates. Here, the figure shows the solid white circles of different sizes ranging from 3 mm to 30 mm. Considering this radius range, the application of a single scaling down on the output data is not possible: the resulting downscaled image would contain errors, and the white pixel centroid would not even be centered compared to the original image. Hence, the algorithm must fully recompute new coordinates in the exact original `Pattern` coordinates on the new resolution system.

During image downscaling, the source image loses pixel property information, and based on the final spatial constraints, it can assume many different possible shapes. Fig. 11b and Fig. 11c show some downscaled shapes of a solid white circle that were obtained using conventional rescaling methods. For TCFVS, shape uniformity, intensity and stability are crucial features to be preserved, therefore, the new shape imposed by our algorithm given in Fig. 11b are considered stable (non-noisy). The solid white circles in Fig. 11c, instead, is not suitable for stimuli experiments due to the potential shape deformation that may occur. We have decided to categorize the possible sizes of the pattern coordinates as given in Tab. 4, to ensure that a stable and uniform shape can be obtained across the `Stimulator`. For instance, a 3 mm

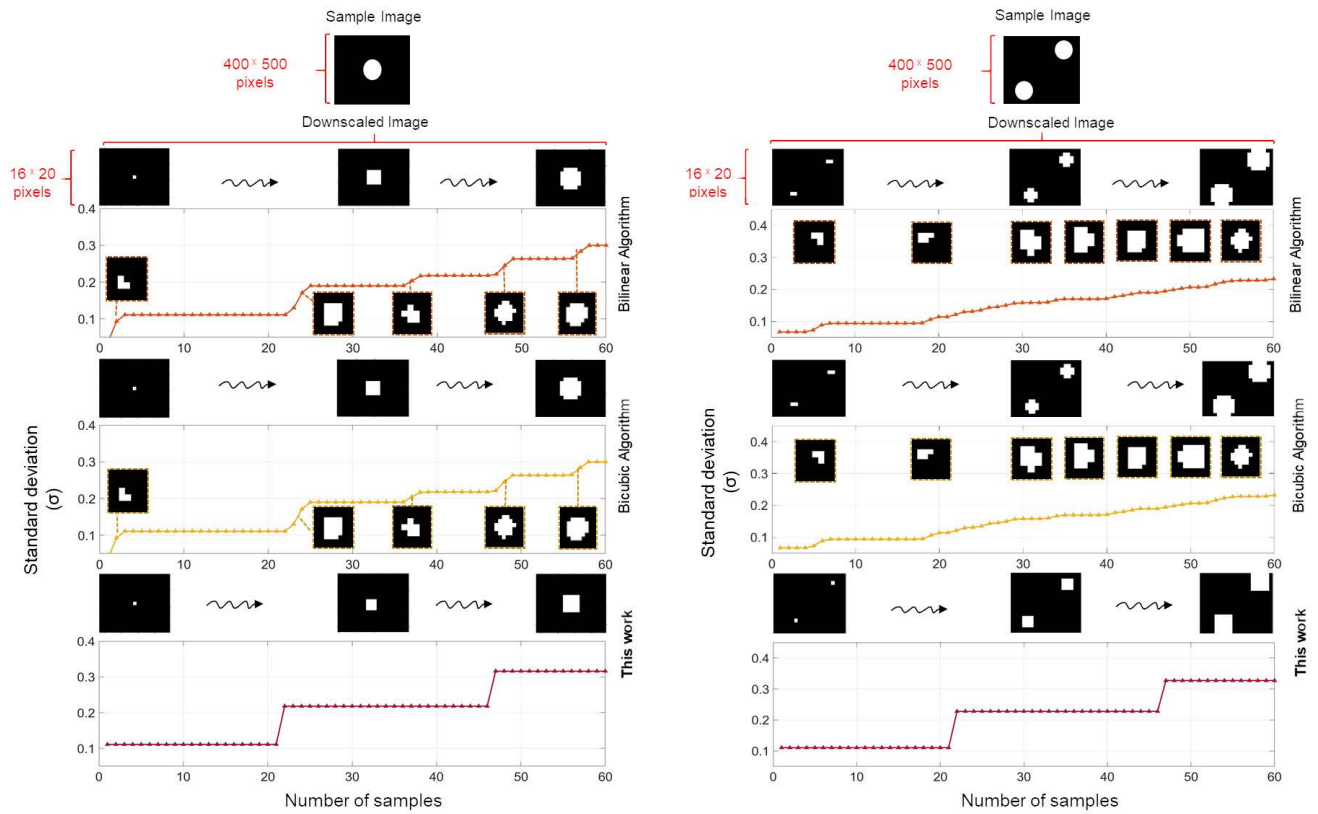


FIGURE 13. (Left) Symmetrical circle and (Right) Two symmetrical circles pattern coordinates and comparison of typical downscale algorithm (Bilinear, Bicubic) with respect to our algorithm, with Standard deviation of the sample image, in all cases to quantify pixel deformation.

TABLE 4. Shape and size categorization of pattern coordinates used in this work.

Marker Dimension size (mm)	Pattern Size (mm)	Number of pixels
3 4 6.4	3-8	1
9.5 14	9-16	4
19 25.4	17-26	9

or 6.4 mm Marker is categorized to a 3-8 mm Pattern size that, in turn, in our algorithm, is mapped to a single pixel on the Stimulator.

A pixel irregularity can directly be linked with standard deviation σ . The standard deviation of a binarized image provides the dispersion of white level intensities I as a measure of the total area of white pixels a (see Fig. 12a) [24]. As the diameter of the solid white circle in a pattern increases, the standard deviation of the sample image also increases steadily, thus identifying the relationship $f(\cdot)$ between the intensity I and the diameter, i.e., $\sigma = f(a)$. Fig. 12b shows the intensity of a sample image that has the highest diameter in three dimensions.

We have used three data sets: symmetrical, asymmetrical, and random solid white circles addressing every pattern categorized in Tab. 4 (e.g., 20 for 3–8 mm, 20 for 9–16 mm, and

20 for 17–26 mm), the actual size of the Vicor Markers, to validate our algorithm. We have systematically analyzed and tested the algorithm (Alg. 1) using the following methods to obtain the best comparative results. These methods involve (i) the increase in the number of circles that can fit in to the 16×20 display without overlapping each other (from one to eight circles), (ii) the dimensional increase of each circle from 3 to 26 mm for every 0.3 mm, giving 60 samples each (from one to four circles), (iii) different data sets of symmetrical, and asymmetrical circles, and (iv) a random image with complex asymmetrical circles. This set of methods provided a meaningful validation of our algorithm. However, to test its reliability and repeatability, we have applied randomly selected trials for the generation of a single recurring result. We present here, in Fig. 13 and 14 only the best cases for pixel distortion to compare with the state-of-the-art downscaling methods (worst cases are not even considered). Observe that the goal of our algorithm was to have a straightforward and distortion-free pixel conversion to be displayed on the Stimulator for the fetuses.

Fig. 13 shows a comparative analysis for symmetrical patterns on a sample image that has one and two circles. The sample images have only one and two solid circles. However, the standard deviation is deterministic. Under each sample image, we provide the comparative results of downscaling using Bilinear, Bicubic, and This work's

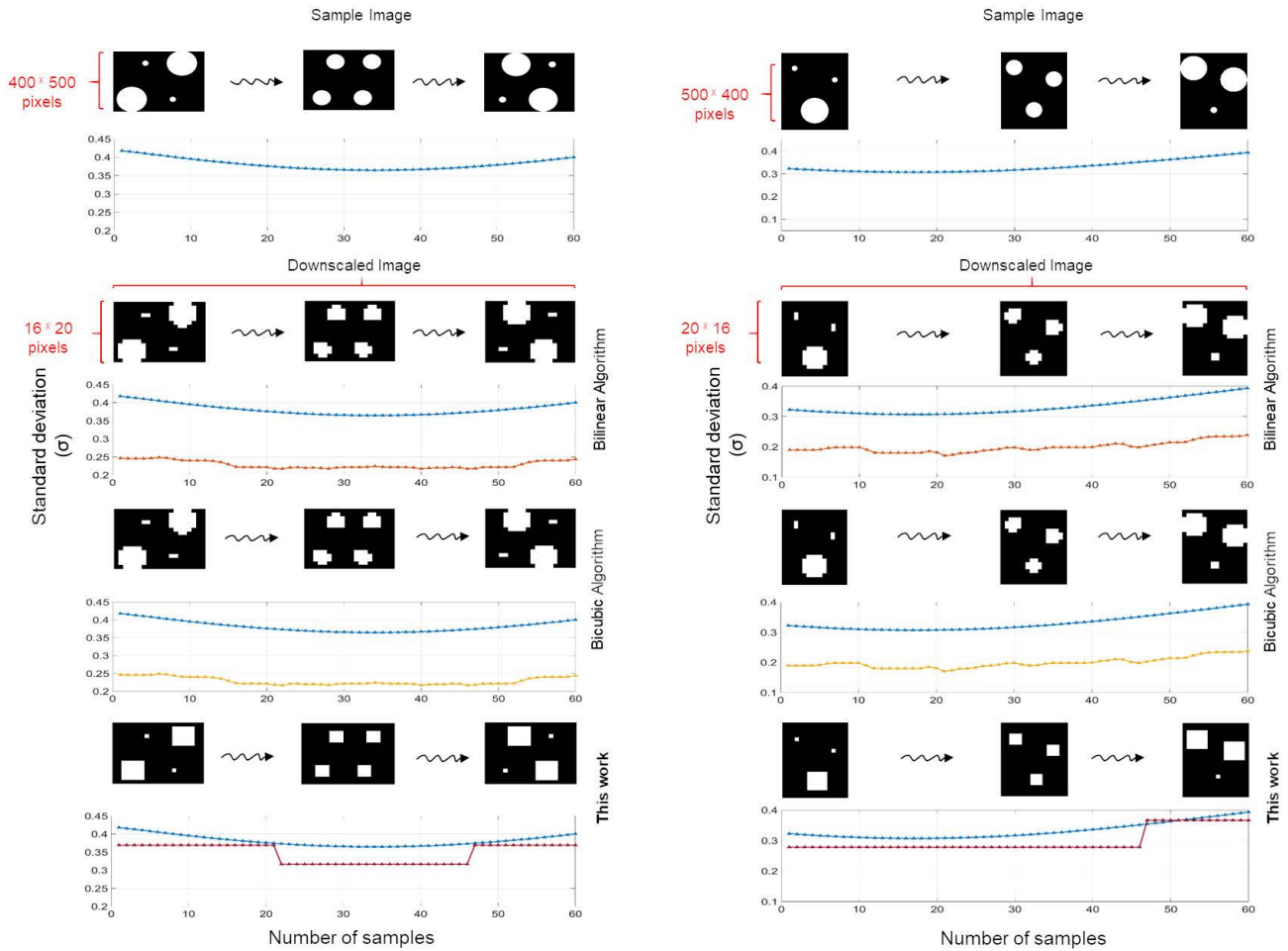


FIGURE 14. (Left) Four asymmetrical circles and (Right) three asymmetrical circles pattern coordinates and comparison of typical downscale algorithm (Bilinear, Bicubic) with respect to our algorithm, with standard deviation of the sample image, in all cases to quantify pixel deformation.

algorithm. By observing the standard deviations of Fig. 13, we can clearly distinguish that conventional algorithms have multiple and irregular plateaus in the standard deviation that indicates pattern deformation that is not suitable for TCFVS application. These constant intervals in the standard deviation are also present in our algorithm, but these are regular and deterministic, and due to the hard Marker dimension mapping given in Tab. 4.

Likewise, Fig. 14 compares asymmetrical patterns standard deviation and pixel deformation at different pattern size parameters, in particular for two pattern types. In this plot, each standard deviation has a superposed curve indicating the upscale image σ , to identify variations and give a more informative representation of the determinism. Normally, the variation between the σ obtained after running the conventional algorithm has an offset compared to the source image because the final image has a smaller pixel size. Using our algorithm that embeds the three-level quantized classification, the variation compared to the source standard deviation is minimized. Moreover, in conventional algorithms, the pixel deformation is near the high-frequency data (pixel information varies fast,

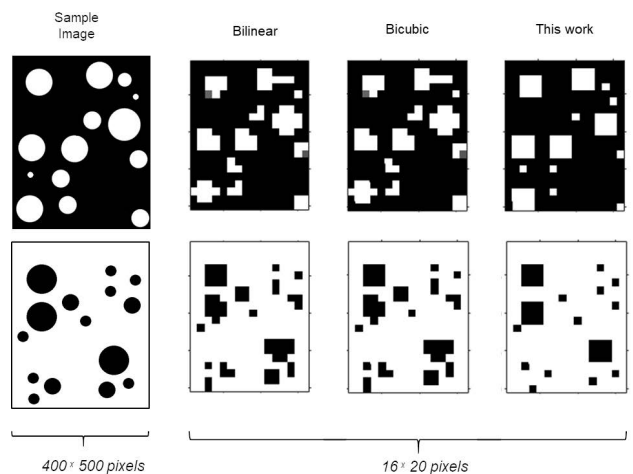


FIGURE 15. Random pattern of a sample image and their subsequent downscaled images.

that is σ has a small but relevant variation compared to its average value), which causes the final shape deformation. The above analysis shows that our algorithm provides a stable and reliable output for our TCFVS hardware.

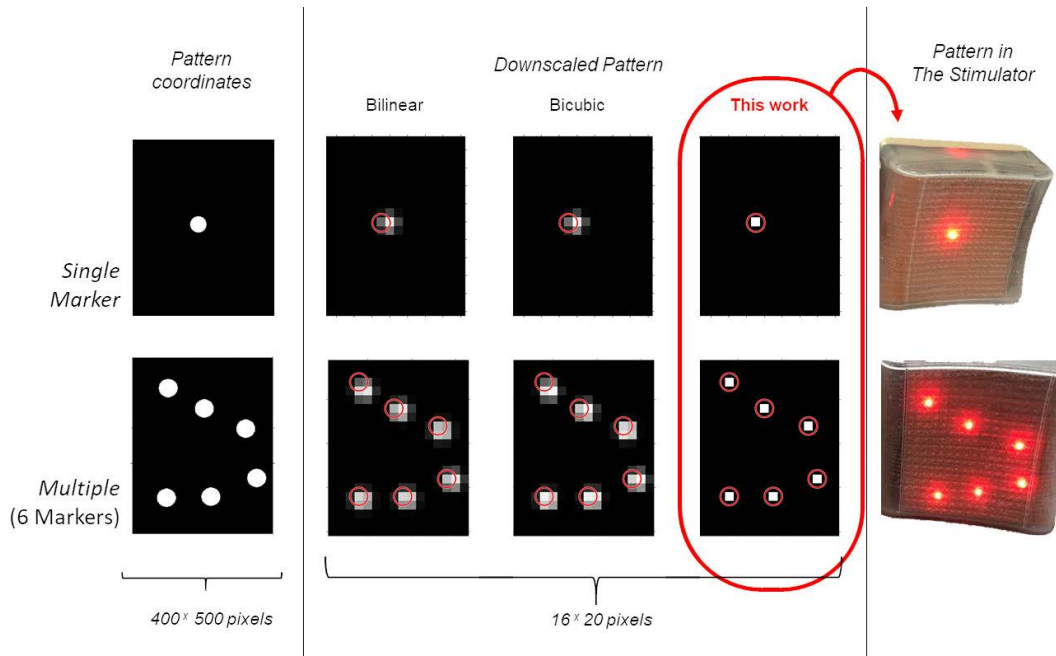


FIGURE 16. Comparison of the output obtained using state-of-the-art Bilinear, Bicubic and this work algorithm from the two image sources Single Marker (top) and the Multiple (6 Markers) (bottom). The output of our pixel remapping technique can be directly used in the TCFVS Stimulator.

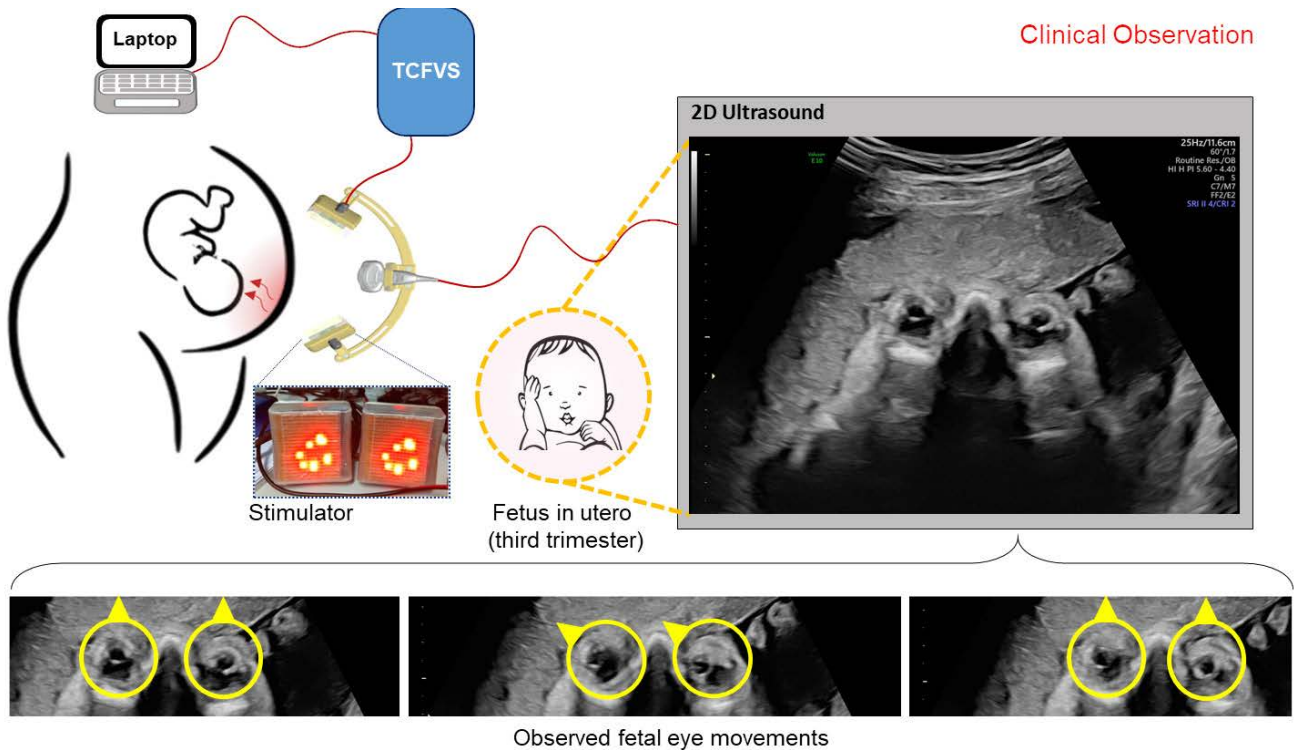
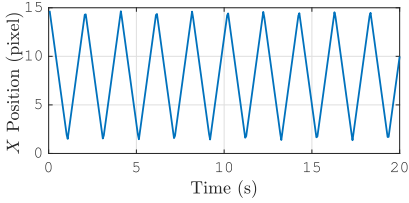
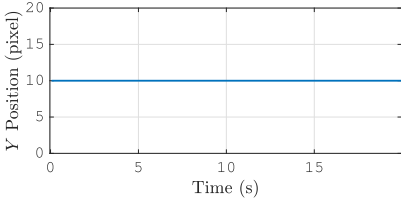
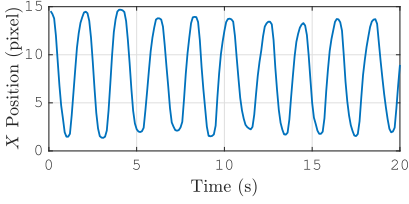
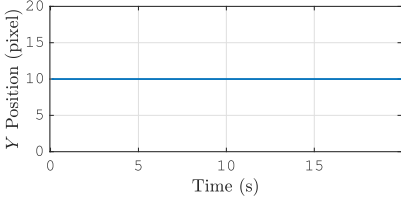
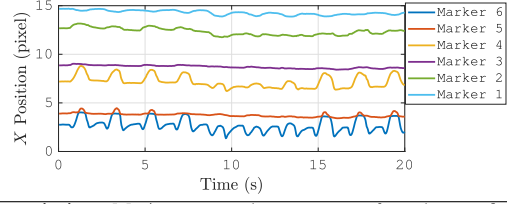
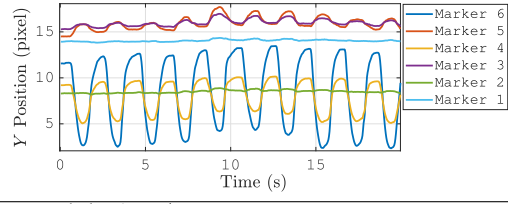
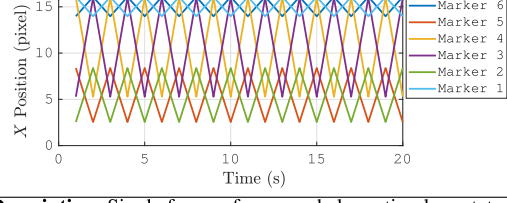
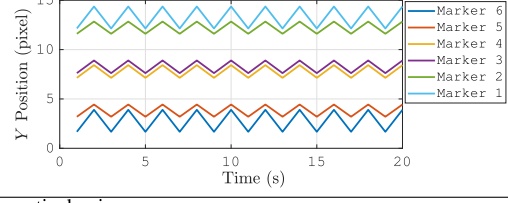


FIGURE 17. Observation of fetal eye-movement on a 30 gestation weeks fetus using a set-up including both 2D Ultrasound and our TCFVS system. The yellow arrows indicate the gaze direction.

Finally, a qualitative comparison of the Bilinear, Bicubic, and This work algorithm applied on the random pattern is shown in Fig. 15. In this context, the

standard deviation is not a meaningful metric because, here, the patterns have solid white circles of various sizes placed at different positions, hence, it is not possible to establish

TABLE 5. TCFVS visual stimulus type, used for fetal observation experiments.

Motion type	Velocity Profile	Horizontal X Plane Profile	Vertical Y Plane Profile
Movement of a Single Marker (see Fig. 16 top)	Constant		
	Description: Software-rendered linear movement of the Marker in the horizontal plane		
Biological			
	Description: Motion-captured linear movement of a human finger in the horizontal plane		
Movement of Multiple (6 Markers) (see Fig. 16 bottom)	Biological		
	Description: Motion-captured movements of two human fingers (open and close) motion		
Constant			
	Description: Single frame of open and close stimulus rotated on its vertical axis		
All stimuli are recorded in an audio-video interleaved format for 20 s at 17.5 frame/s.			

a direct relationship with σ . The classical algorithm outputs generate patterns with significant noise and the impossibility to identify each Pattern coordinates position after downsampling. In our algorithm, thanks to the full remapping of each centroid in Pattern coordinates, we can guarantee a noiseless correspondence with the original image.

Fig. 16 shows patterns obtained in the TCFVS using one marker (upper row) and six markers (lower row). To verify the efficiency of our patterning technique, we compared the output obtained with the same Vicon files using the conventional algorithms already discussed. From left to right, we report the rescaling techniques and their corresponding outputs. Conventional algorithms are simple, fast, and near-optimal. However, they cannot be used to flexibly impose a pixel size selection because the resulting centroids have a relative positioning error (refer to the red circles and their shift in the h and v space). On the other hand, when the

high-resolution motion data is processed using our algorithm, the centroids and the resulting markers spatial distribution are maintained, and the image can be directly rendered with the TCFVS hardware.

To assess the device’s correct operation, first, we considered a movement of marker(s) at a constant velocity, i.e., a computer-generated pixel that moves at a constant velocity (e.g., see the top marker in Fig. 16). Second, we considered a biological movement, i.e., the outcome of the motion capture system that acquires human finger(s) movements as a stimulus. Together, we generated a curated visual stimulus dataset for visual stimulus experiments. Tab. 5 illustrates the types of visual stimulus and their corresponding profile used for observing fetal reactions in real experiments. The motion involves (i) the oscillating Single Marker in the horizontal plane at a constant velocity (16 pixels/s), (ii) the motion-captured version of a Single Marker from the

TABLE 6. Visual experiments parameters of state-of-the-art systems compared to those of TCFVS (in the present experiment).

Reference	Light Source	Beam Diameter (mm)	Wavelength (nm)	Number of Sources	Power per Source	Total Area (cm ²)	Observation Method	Display Description
[2], [26]	LASER	2	650	3	0.5–5 mW	–	4D Ultrasound	Static configuration
[27]	LED	3	640	12	3 W	12.25	4D Ultrasound	Static configuration
[28]	LED	3	640	50	2.5 W	20	fMRI	Static configuration
This work	LED	1.2	640	320	84 mW	50.4	2D Ultrasound	Complex Visual Stimuli

human finger swaying across the horizontal plane, which represents a biological motion (one can observe its velocity compared to mechanical motion), (iii) the motion-captured version of the Multiple (6 Markers) placed on the index finger and thumb to perform an opening and closing action, and (iv) the rotation of a single frame of open and close stimulus rotated in its vertical axis at every second.

Fig. 17 shows a schematic illustration of an example in uterus visual stimulation by TCFVS in combination with a 2D Ultrasound. The figure illustrates the simple three-stage procedure to record fetal responses to visual stimulation. The experimenter positions the probe, selects the stimulation file in the laptop (here, the experimenter can choose a motion profile given in Tab. 5), and visualizes the fetal response (eye movement) on the 2D Ultrasound. This procedure to determine the gaze direction in fetuses is well established and based on the lens orientation. Indeed, in the 2D Ultrasound, the lens of the eyes can be distinguished as white circles (see Fig. 17) within the hypochoic eyeball, and eye movements can be relatively detected [25]. This procedure to determine the gaze direction in fetuses is well established and based on the lens orientation. Indeed, in the 2D Ultrasound, the lens of the eyes can be distinguished as white circles (see Fig. 17) within the hypochoic eyeball, and eye movements can be relatively detected [25]. We predict that (i) the so-determined number of eye movements will be generally higher during visual stimulation with TCFVS compared to no-visual stimulation; (ii) during visual stimulation with TCFVS, the proportion of eye movement towards the displayed stimulus will be higher compared to the proportion of eye movements performed away from the stimulus. To test these predictions, the planned study using TCFVS in combination with the 2D Ultrasound will include a baseline condition (no visual stimulation).

V. DISCUSSION

To the best of our knowledge, existing approaches do not permit the presentation of complex shapes and motion patterns to the fetus. Tab. 6 compares existing devices parameters available to visual stimuli through the maternal abdomen. In [2], [26], a LASER for visual stimulus experiments is used. Three light sources can send fixed static patterns as a visual stimulus to the fetus. However, these patterns are fixed (i.e., the LASER can be simply activated or deactivated).

Furthermore, in [27], a floating LED array for stimulus experiments is implemented. This floating array offers the

flexibility to change the position of 12 LEDs to create any static shape as a visual stimulus. However, to send different patterns as a visual stimulus, it is necessary to change the positioning of the LEDs physically.

Finally, in [28], an endoscopic probe that uses 50 LEDs to send brightness as a visual stimulus is implemented. However, the LEDs are a rigid element, which can either be activated or deactivated with no possibility of rendering different patterns. Here, in TCFVS, the hardware and the associated software toolchain can emulate any shape or render any biological or mechanical pattern on its Stimulator. All the devices in the literature, which in any case do not provide the capabilities of TCFVS that can easily stimulate random mechanical movements (as they do not provide a fixed frame display), but they do not support biological motion rendering.

In our system, the size of each light source (LEDs) is significantly small (i.e., 1.2 mm), and stacking them on a flexible PCB with a translucent screen permits light dispersion on a bigger space (50.4 cm² overall area). The AUX_DISP module in the TCFVS system regulates the light sources to provide a constant light intensity on the Stimulator. Unlike the existing setups, a significant advantage of the platform is that, through the UI, it allows the switching between the stimuli for any need in the experiment without ad-hoc mechanical intervention. Mechanical intervention can ideally provide ultra-fine adjustment of fixed light sources, but it is strongly unpractical and not easily automatable. On the other hand, the display must be manufactured with a given size, weight, and resolution: the current Stimulator is constrained to a 16 × 20 pixels resolution. This intrinsic disadvantage of fixed resolution is tackled by the capability of filtering source visual stimulations with the algorithms presented herein. Lastly, TCFVS is the first of its kind to be capable of automatically rendering programmed dynamic stimuli.

VI. CONCLUSION

We have presented the design of a transcutaneous fetal visual stimulator to be used to assess the visual perceptual ability of the fetuses. We have designed both the hardware of the device, including mechanics and electronics, and the associated software toolchain to automatically convert generic mechanical motion or motion-captured sequence into a format that is suitable for the rendering on the device. We have validated the software and hardware to assess the generation of visual stimuli. Moreover, a fetus at 30 gestation weeks is

shown to provide specific reactions to visual stimuli, hence yielding a first effectiveness proof of our architecture.

ACKNOWLEDGMENT

Written informed consent was obtained from all the participants prior to the recordings. The authors would like to thank the participants and their families for their efforts to participate in this study, and also would like to thank the hospital staff for their support with the scientific data collection and Davide Dellepiane, IIT-EDL, for device cabling and assembly support.

REFERENCES

- [1] K. Dunn, N. Reissland, and V. M. Reid, "The functional foetal brain: A systematic preview of methodological factors in reporting foetal visual and auditory capacity," *Develop. Cognit. Neurosci.*, vol. 13, pp. 43–52, Jun. 2015.
- [2] V. M. Reid, K. Dunn, R. J. Young, J. Amu, T. Donovan, and N. Reissland, "The human fetus preferentially engages with face-like visual stimuli," *Current Biol.*, vol. 27, no. 12, pp. 1825–1828, 2017.
- [3] G. Johansson, "Visual perception of biological motion and a model for its analysis," *Perception Psychophys.*, vol. 14, no. 2, pp. 201–211, 1973.
- [4] V. M. Reid and K. Dunn, "The fetal origins of human psychological development," *Current Directions Psychol. Sci.*, vol. 30, no. 2, pp. 144–150, Apr. 2021.
- [5] F. Simion, L. Regolin, and H. Bulf, "A predisposition for biological motion in the newborn baby," *Proc. Nat. Acad. Sci. USA*, vol. 105, no. 2, pp. 809–813, Jan. 2008.
- [6] *Biocompatible Clear MED 610*. Accessed: Sep. 18, 2018. [Online]. Available: <https://www.stratasys.com/-/media/files/material-spec-sheets/biocompatible-data-sheets-c.zip>
- [7] *Biocompatible ULTEM 9085*. Accessed: Sep. 18, 2018. [Online]. Available: https://www.stratasys.com/-/media/files/material-spec-sheets/MDS_FDM_ULTEM9085_1020a.pdf
- [8] M. Del Giudice, "Alone in the dark? Modeling the conditions for visual experience in human fetuses," *Develop. Psychobiol.*, vol. 53, no. 2, pp. 214–219, Mar. 2011.
- [9] A. R. Young, "Chromophores in human skin," *Phys. Med. Biol.*, vol. 42, no. 5, pp. 789–802, May 1997.
- [10] K. J. Schlager and R. W. Ignatius, "LED-array light source for medical therapy," in *Medical Lasers and Systems II*, vol. 1892. Bellingham, WA, USA: SPIE, 1993, pp. 26–35.
- [11] P. Bartczak, A. Gebejes, P. Falt, and M. Hauta-Kasari, "An LED-based tunable illumination for diverse medical applications," in *Proc. IEEE 29th Int. Symp. Comput.-Based Med. Syst. (CBMS)*, Jun. 2016, pp. 292–293.
- [12] *Kingbright 1.6 mm×0.8 mm SMD Chip LED Lamp*. Accessed: Sep. 18, 2018. [Online]. Available: https://eu.mouser.com/datasheet/2/216/APTD1608SECK_J3_PF-472767.pdf
- [13] *Build High-Density, High-Refresh Rate, Multiplexing LED Panel With TLC5958*. Accessed: Jun. 25, 2020. [Online]. Available: <https://www.ti.com/lit/ug/slvauf0/slvauf0.pdf>
- [14] *MYIR Z-Turn Board*. Accessed: Sep. 18, 2018. [Online]. Available: <http://www.myirtech.com/download/Zynq7000/Z-turnBoard.pdf>
- [15] *XILINX VIVADO*. Accessed: Sep. 18, 2018. [Online]. Available: <https://www.xilinx.com/products/design-tools/vivado.html>
- [16] *AMBA Specifications—Arm Developer*. Accessed: Aug. 13, 2020. [Online]. Available: <https://developer.arm.com/architectures/system-architectures/amba/specifications/>
- [17] *Vicon Motion Systems*. Accessed: Apr. 25, 2021. [Online]. Available: <https://www.vicon.com/>
- [18] D. Lewkowicz and Y. Delevoe-Turrell, "Real-time motion capture toolbox (RTMocap): An open-source code for recording 3-D motion kinematics to study action–effect anticipations during motor and social interactions," *Behav. Res. Methods*, vol. 48, pp. 366–380, 2016.
- [19] J. Peng, A. Loew, O. Merlin, and N. E. C. Verhoest, "A review of spatial downscaling of satellite remotely sensed soil moisture," *Rev. Geophys.*, vol. 55, no. 2, pp. 341–366, 2017.
- [20] S. H. W. Scheres, R. Núñez-Ramírez, C. O. S. Sorzano, J. M. Carazo, and R. Marabini, "Image processing for electron microscopy single-particle analysis using XMIPP," *Nature Protocols*, vol. 3, no. 6, pp. 977–990, Jun. 2008.
- [21] A. B. Szczotka, D. I. Shakir, M. J. Clarkson, S. P. Pereira, and T. Vercauteren, "Zero-shot super-resolution with a physically-motivated downsampling kernel for endomicroscopy," *IEEE Trans. Med. Imag.*, vol. 40, no. 7, pp. 1863–1874, Jul. 2021.
- [22] W. Sun and Z. Chen, "Learned image downscaling for upscaling using content adaptive resampler," *IEEE Trans. Image Process.*, vol. 29, pp. 4027–4040, 2020.
- [23] P. Hough, "Method and means for recognizing complex patterns," U.S. Patent 3 069 654 A, Mar. 25, 1960. [Online]. Available: <http://www.google.com/patents/US3069654/>
- [24] J. Lázaro, A. Cano, P. Fernández, and Y. Pompa, "Sensor for distance measurement using pixel grey-level information," *Sensors*, vol. 9, no. 11, pp. 8896–8906, Nov. 2009.
- [25] M. Inoue, T. Koyanagi, H. Nakahara, K. Hara, E. Hori, and H. Nakano, "Functional development of human eye movement in utero assessed quantitatively with real-time ultrasound," *Amer. J. Obstetrics Gynecol.*, vol. 155, no. 1, pp. 170–174, 1986.
- [26] T. Donovan, K. Dunn, A. Penman, R. J. Young, and V. M. Reid, "Fetal eye movements in response to a visual stimulus," *Brain Behav.*, vol. 10, no. 8, pp. 1–6, Aug. 2020.
- [27] N. Reissland, R. Wood, J. Einbeck, and A. Lane, "Effects of maternal mental health on fetal visual preference for face-like compared to non-face like light stimulation," *Early Hum. Develop.*, vol. 151, Dec. 2020, Art. no. 105227.
- [28] J. Fulford, S. H. Vadeyar, S. H. Dodampahala, R. J. Moore, P. Young, P. N. Baker, D. K. James, and P. A. Gowland, "Fetal brain activity in response to a visual stimulus," *Hum. Brain Mapping*, vol. 20, no. 4, pp. 239–245, Dec. 2003.



KARTHIKEYAN KALYANASUNDARAM BALASUBRAMANIAN (Member, IEEE) received

the bachelor's degree in engineering from Anna University, Chennai, India, in 2006, the master's degree from SRM University, Chennai, in 2009, and the Ph.D. degree from the Vellore Institute of Technology, Chennai, in 2019, all in electrical and electronics engineering. From 2018 to 2019, he was a Visiting Research Assistant with the Electrical Engineering Department, University of New South Wales (UNSW), Sydney, Australia. He is currently a Postdoctoral Research Fellow with the Center for Human Technology (CHT-IIT), Istituto Italiano di Tecnologia, Genova, Italy. His research interests include developing systems for neuroscience, medical robotics, and soft robots. He has authored or coauthored several international publications and has two patents.



FRANCESCO DIOTALEVI received the M.S. and

Ph.D. degrees in electronic engineering from the University of Genova, Italy, in 1996 and 2001, respectively. He was involved in analog microelectronic supervised learning systems with emphasis in silicon implementation of neural networks. In 2001, he joined the Accent SpA., a joint venture between ST Microelectronics and Cadence Design System, as a Senior Consulting Engineer, where he was an ASIC Designer for several digital designs in different fields of applications, such as automotive, fingerprint sensors, and multimedia. In 2009, he joined the TeleRobotics and Applications, Department of the Istituto Italiano di Tecnologia, Genova. Since 2011, he has been with the Electronic Design Laboratory. He is currently interested in low-power computing systems for mobile robots and humanoids, FPGA design, and embedded systems.



created devices for various applications in robotics, sensing, rehabilitation, medical, and data communication.

CLAUDIO LORINI received the degree in electronic engineering from the Università degli studi di Genova (Unige), in 1996. In 2000, he received qualification to practice the engineering profession from the Ministero dell'università e della ricerca scientifica. His working experience started, in 1988, covers the design of devices in the industrial, automation, and medical fields. Since 2007, he has been with the Fondazione Istituto Italiano di Tecnologia, as a Design Engineer, where he



and coauthored more than 50 publications in peer-reviewed journals.

ANDREA CAVALLO received the master's degree in clinical psychology from the University of Padua, in 2008, and the Ph.D. degree in neuroscience from the University of Turin, in 2013. He is currently an Associate Professor with the Department of Psychology, University of Turin. His research interest includes the processes that transform external sensory information into the corresponding internal motor representation (i.e., motor cognition). As a Principal Investigator, he is currently

working on new approaches to investigate motor components of dyadic interactions in both clinical and non-clinical populations. He has authored



healthy fetuses, and in children, both typically developing and those with an autism spectrum disorder.

NOVELLA PRETTI received the M.S. degree in psychology and neuroscience from the University of Torino, Italy, in 2016. She is currently pursuing the Ph.D. degree with the Cognition Motion and Neuroscience (C'MoN) Research Unit, Italian Institute of Technology (IIT), Genova. Her research aims to identify and quantify motor patterns from the fetal period through postnatal development. Within the Unit, she is involved with several studies assessing movement kinematics in



Fetal Medicine Unit, Poissy University Hospital, Paris, France, in 2006. In 1991, he joined the OBGYN Department, Federico II, University of Naples, Italy, to work on high-risk pregnancy, fetal medicine, and gynecologic oncology. Since 2013, he has been the Head of the Fetal Medicine and Surgery Unit, Gaslini Children's Hospital Genoa, Italy. He is a member

DARIO PALADINI received the Doctor of Medicine degree (*summa cum laude*), in 1986, and he specialized in obstetrics and gynecology, in 1990. Both during and after his studies, he participated in various training programs that are Fetal Echocardiography—Guy's Hospital London, U.K., in 1988, Gynecologic Oncology—Istituto Nazionale Tumori, Milano, Italy, from 1990 to 1994, Queen Elizabeth Hospital, Gateshead, U.K., in 1992, and Fetal Surgery—

of major National and International societies of OBGYN and Ultrasound. He has been contributing to the development and updates of national (SIEOG) and international (ISUOG) societies of OBGYN Ultrasound. For ISUOG, he is the Board Member, the Chair of the Education Committee, the Chair of the Courses Committee, and the Chair of the Task Forces on Neurosonography and CHD-CNS Lesions. He has taught and spoken at 100 of training courses, and congresses worldwide. He was an External Counselor for the set-up of the Fetal Medicine Unit, Dubai Hospital, Dubai, United Arab Emirates (UAE), from 2018 to 2019. He has authored more than 200 articles in peer-reviewed high-impact factor journals. He has received the Top award in the world for training in OBGYN Ultrasound, and he received ISUOG Stuart Campbell Award, in 2011. Since 2019, he has been the Chair of the Stuart Campbell Award.



equipment, superconductor magnets, and robotics for research and rehabilitation). Since 2013, he has been a Senior Technician at IIT, and until recently, in 2018, he is also an Adjunct Professor with the Università degli studi di Genova (Unige), teaching industrial technical drawing.

DIEGO TORAZZA received the degree in mechanical engineering from the Università degli studi di Genova (Unige), in 2004. In 2007, he acquired the Italian State qualification for Mechanical Engineer activity (Section B). His working experience began, in 2004, as a Mechanical Designer for various research institutes and private companies (INFN, Istituto Italiano di Fisica Nucleare, ASG Superconductors, and Italian Institute of Technology) in different fields (nuclear physics research



by an ERC Proof-of-Concept Grant (2018–2020).

CRISTINA BECCHIO received the Philosophy degree (*summa cum laude*) and the Ph.D. degree in cognitive science from the University of Turin, in 2000 and 2001, respectively. In 2004, she moved to cognitive neuroscience as a Postdoctoral Researcher and had since been working on motor cognition. In 2011, she was appointed as an Associate Professor, and in 2015, as a Full Professor with the University of Turin. In 2014, she joined the Italian Institute of Technology as a PI of the

Unit Cognition, Movement and Neuroscience. From 2020 to 2021, she was the Coordinator of the Center for Human Technologies. Since 2022, she has been a Professor in cognitive neuroscience with the Department of Neurology, University Medical Center Hamburg-Eppendorf. Her research interests include the control and perception of body movements during human social interaction, both in typical and atypical populations. In this area, she was awarded an ERC Consolidator Grant (2013–2018), followed



and coauthor of more than 90 publications and two international patents.

MARCO CREPALDI (Member, IEEE) received the Engineering degree (*summa cum laude*) and the Ph.D. degree in electronic engineering from the Politecnico di Torino (PoliTo), Turin, Italy, in 2005 and 2009, respectively. In 2008, he was a Visiting Scholar with the Electrical Engineering Department, Columbia University, New York. After the Ph.D. degree, he worked as a Postdoctoral Researcher with the VLSI-Laboratory, Electrical Engineering Department, PoliTo, and then as a Postdoctoral Researcher with the Former Istituto Italiano di Tecnologia@PoliTo—Center for Space Human Robotics (IIT-CSHR). He is currently the Coordinator of the Electronics Design Laboratory (edl.iit.it), IIT Center for Human Technologies, Genova. His research interests include the development of all-digital impulse-radio ultra-wide band (IR-UWB) systems and electronic systems design. He is the author